A systematic RNA interference screen reveals a cell migration gene network in *C. elegans*

Erin J. Cram, Hongyu Shang and Jean E. Schwarzbauer*

Department of Molecular Biology, Princeton University, Princeton, NJ 08544-1014, USA

*Author for correspondence (e-mail: jschwarz@princeton.edu)

Accepted 21 September 2006
Journal of Cell Science 119, 4811-4818 Published by The Company of Biologists 2006
doi:10.1242/jcs.03274

Summary

Cell migration is essential during embryonic development and tissue morphogenesis. During gonadogenesis in the nematode *Caenorhabditis elegans*, migration of the distal tip cells forms two U-shaped gonad arms. Malformation results if the distal tip cells stop prematurely or follow an aberrant path, and abnormalities are easily visualized in living nematodes. Here we describe the first comprehensive in vivo RNA interference screen for genes required for cell migration. In this non-biased screen, we systematically analyzed 16,758 RNA-interference depletion experiments by light microscopy and identified 99 genes required for distal tip cell migration. Genetic and physical interaction data connect 59 of these genes to form a cell migration gene network that defines distal tip cell migration in vivo.

Supplementary material available online at
http://jcs.biologists.org/cgi/content/full/119/23/4811/DC1

Key words: Cell migration, *Caenorhabditis elegans*, RNAi, Gonad

Introduction

Cell migration plays a central role in tissue development and for processes such as wound healing and cancer metastasis. The nematode *C. elegans* is ideal for visualizing cell migration in vivo because of limited morphological variability and a translucent body (Shakir and Lundquist, 2005). Gonad morphogenesis occurs post-embryonically via migration of two distal tip cells (DTCs), specialized leader cells that develop at each end of the gonad primordium and migrate during larval development (Lehmann, 2001). The two DTCs migrate in opposite directions along the ventral basement membrane, with appropriate cues they turn toward the dorsal side, and then turn again to migrate back toward the midline, resulting in a mirror-image U-shaped gonad (Fig. 1B). Several classes of genes have been shown to participate in migration of the DTC including an integrin cell adhesion receptor (Baum and Garriga, 1997; Lee et al., 2001), the netrin guidance system (Merz et al., 2001), cell death and/or Rac-GTPase signaling components (Reddien and Horvitz, 2000) and matrix metalloproteinases (Hesselson et al., 2004; Kubota et al., 2004; Nishiwaki et al., 2004). Despite these advances, our understanding of the extracellular interactions and intracellular mechanics of DTC migration remains incomplete.

In this study, we used a genome-wide RNA interference (RNAi) approach to identify a set of 99 genes required for DTC migration, including many novel factors not previously linked to cell migration. Orthologs of migration genes from mammalian and other systems as well as known DTC migration genes were also identified. One of these genes, *ppn-1*, encodes the papilin ortholog which we show to be required very early in gonadogenesis. Assembly of a cell migration gene network demonstrates that at least 59 of these factors cooperate to control cell migration. The interconnected genes in this network provide a foundation for future study of cell migration in the nematode and in other systems.

Results and Discussion

To identify genes required for DTC migration, we have analyzed a library of bacterial strains expressing double-stranded RNA that targets >80% of *C. elegans* open reading frames (Kamath and Ahringer, 2003). To bypass the embryonic lethality associated with many genes involved in cell migration and to allow observation of late larval and adult phenotypes, nematodes were cultured on individual bacterial strains from hatching to adulthood and young adults were screened for DTC migration defects using light microscopy. A two-step visual screen was applied (Fig. 1A). The primary low-magnification screen identified clear patches that result from displacement of the intestine because of inappropriate turns of the gonad arms or gonad distension (Nishiwaki, 1999; Cram et al., 2003). This screen is stringent; of the 16,758 bacterial strains tested, only 3% or 503 strains resulted in some clear patches (Table S1, supplementary material). We then examined these genes in a secondary screen in which the penetrance and types of gonad migration defects were documented by differential interference contrast (DIC) Nomarski microscopy of young adult animals (P0). When viable, progeny (F1) animals were also scored 48 hours after hatching. In some cases, depletion resulted in additional phenotypes, but these did not preclude scoring of the DTC migration defect. 99 RNAi clones produced reproducible DTC migration defects in ⩾30% of distal tip cells scored (Table 1). Additional information about each of these genes including putative protein functions, conserved motifs, and homologs can be found in Table S2, supplementary material.

The results of our screen verified that our method is effective at identifying cell migration regulators, because we isolated genes previously known to be involved in DTC migration. For

Table 1. Genes required for DTC migration

Sequence name	Locus	Functional class	Description	P0 defect	*n*	F1 defect	*n*
B0511.8		Metabolism	Mitochondrial 28S ribosomal protein S30	0.53	66		
C01G8.5	erm-1	Cell architecture	ERM family of cytoskeletal linkers	0.32	74		
C02C6.1	dyn-1	Cell architecture	Vacuolar sorting protein dynamin	0.80	52		
C02F4.1	ced-5	Cell architecture	DOCK180 scaffold protein	0.38	98	0.70	86
C06G3.10	cogc-2	Unknown	Conserved oligomeric Golgi complex component	0.54	168	0.40	80
C09G12.8†	ced-10	Signaling	Ras-related small GTPase, Rac	0.58	60	0.65	46
C09H10.7		Unknown	Unknown	0.08	66	0.96	98
C15F1.3	tra-2	Unknown	Transmembrane receptor – role in sex determination	0.17	98	0.64	44
C16C10.6		Unknown	Unknown	0.39	130		
C24D10.4		Unknown	Unknown	0.05	100	0.46	92
C27H6.2	ruvb-1	DNA binding	DNA helicase, TBP interacting protein	0.47	64		
C28C12.8	hlh-12	Transcription factor	Helix-loop-helix transcription factor	0.80	92	0.50	144
C36E8.5*	tbb-2	Cell architecture	Beta tubulin	0.88	56		
C37C3.6	ppn-1	ECM	Papillin/ thrombospondin repeat protein	1.00	146		
C43H6.9	glr-7	Other	Glutamate receptor	0.09	90	0.38	78
C47B2.3*	tba-2	Cell architecture	α-Tubulin	1.00	30		
C47E12.4	pyp-1	Metabolism	Nucleosome remodeling factor	0.41	56		
C47E8.7	unc-112	Cell architecture	Homologous to Mig-2 – contains ERM and PH domains	0.22	110	0.37	30
C53B4.1		Other	Organic cation transporter	0.14	96	0.32	84
C56C10.8	icd-1	Transcription factor	Transcription factor, subunit of RNA polymerase II	0.50	58		
D1037.4	rab-8	Signaling	Rab-related protein of the Ras GTPase superfamily	0.45	80	0.40	72
D1069.3		Unknown	Unknown	0.34	68	0.83	116
F01G12.5	let-2	ECM	α2 Type IV collagen	0.88	26		
F11A3.2		Protein synthesis	Translation initiation factor 2B	0.42	96		
F14F3.1	vab-3	Transcription factor	Transcription factor, related to eyeless	0.54	90	0.58	98
F20H11.2	nsh-1	DNA binding	Nuclear helicase MOP-3/SNO (DEAD-box superfamily)	0.27	90	0.45	94
F21C3.5		Cell architecture	Prefoldin subunit 6, KE2 family chaperone	0.32	68	0.47	34
F25G6.2		Unknown	Scaffold protein for polyadenylation factors	0.56	88		
F25H8.3	gon-1	Degradation/protease	ADAMTS metalloprotease	1.00	70		
F26E4.8*	tba-1	Cell architecture	α-Tubulin	0.93	72		
F26F4.11		RNA synthesis	RNA polymerase subunit	0.39	84		
F28D1.10	gex-3	Signaling	Nck associated protei	0.38	82		
F32D1.10	mcm-7	Cell cycle	DNA replication licensing factor, MCM7 component	0.30	137		
F32D1.2		Metabolism	Mitochondrial ATP synthase	0.41	106		
F35G12.8	smc-4	Nucleic acid binding	Chromosome condensation complex–Condensin	0.58	80		
F40F11.2		Unknown	Unknown	0.76	79		
F44C4.4	gon-14	Unknown	Unknown	0.15	98	0.63	90
F44F4.11*	tba-4	Cell architecture	α-Tubulin	1.00	27		
F49D11.1	prp-17	RNA synthesis	Splicing factor	0.34	70		
F54G8.3	ina-1	Cell architecture	α Integrin	0.33	84	0.26	78
F55C7.7	unc-73	Signaling	Guanine nucleotide exchange factor Trio	0.32	62	0.19	64
F55F10.1		Unknown	AAA ATPase enzyme	0.22	110	0.32	78
F56A3.3	npp-6	Cell architecture	Nuclear pore complex	0.46	92		
F56B3.8		Protein synthesis	Mitochondrial/chloroplast ribosomal protein L2	0.36	94	0.37	104
F57C7.3†	sdn-1	Signaling	Transmembrane HSPG syndecan	0.28	80	0.40	82
F57H12.1	arf-3	Signaling	GTP-binding ADP-ribosylation factor	0.72	80		
F58A4.11	gei-13	Transcription factor	Forkhead transcription factor	0.25	92	0.35	51
F58A4.8	tbg-1	Cell architecture	γ-Tubulin	0.26	76	1.00	77
F59A2.1	npp-9	Cell architecture	Nuclear pore complex/Ran-binding protein	0.35	86		
H06I04.3		Metabolism	Putative SAM-dependent rRNA methyltransferase	0.49	142		
K01G5.7*	tbb-1	Cell architecture	β-Tubulin	1.00	54		
K06H7.6	apc-2	Cell cycle	Anaphase-promoting complex (APC), subunit 2	0.11	92	0.76	112
K07E12.1	dig-1	ECM	Matrix protein with FNIII, VWF, Ig domains	0.23	176	0.34	212
K09B11.9			Intracellular protein transport	0.26	86		
M03D4.1	zen-4	Cell architecture	Kinesin-like protein	0.66	61		
M03F4.2*	act-4	Cell architecture	Actin	0.94	36		
M03F4.3	tag-126	Signaling	7TM receptor	0.20	94	0.30	82
M05B5.5†	hlh-2	Transcription factor	Helix-loop-helix transcription factor	0.97	68		
M106.1	mix-1	Nucleic acid binding	Chromosome condensation complex, condensin	0.70	68		
M6.1	ifc-2	Cell architecture	Intermediate filament protein	0.29	82	0.33	84
R02F2.7		Unknown	Unknown	0.43	98		
R07G3.1	cdc-42	Signaling	Ras-related small GTPase, Rho type	0.49	74		
R08D7.2		Unknown	Unknown	0.11	96	0.91	76
R10A10.2	rbx-2	Degradation/protease	SCF ubiquitin ligase Ring-box protein	0.15	34	0.47	62
R10E11.1	cbp-1	Nucleic acid binding	CREB-binding protein	0.76	126		
R53.6		Unknown	DNA replication	0.24	72	0.79	95
T04A8.6		Nucleic acid binding	Nucleolar RNA-binding protein NIFK	0.36	88		
T04C12.6*	act-1	Cell architecture	Actin	0.89	44		
T05C12.7	cct-1	Protein synthesis	Chaperonin complex component, TCP-1 α subunit	0.44	36		
T09A5.10	lin-5	Cell cycle	Coiled-coil component of spindle	0.47	125		

Table 1. Continued

Sequence name	Locus	Functional class	Description	P0 defect	*n*	F1 defect	*n*
T09A5.6	mdt-10	Transcription factor	Transcription factor, subunit of RNA polymerase II	0.15	88	0.43	101
T09E8.1		Unknown	Similar to myosin heavy chain	0.73	96	0.64	88
T13H5.4		RNA synthesis	Splicing factor	0.35	54		
T22F3.4*	rpl-11.1	Metabolism	60S ribosomal protein L11	0.73	110	0.86	7
T23B12.7	dnj-22	Unknown	Molecular chaperone DNAJ	0.24	147	0.56	71
T23F6.4	rbd-1	Nucleic acid binding	RNA-binding protein (RRM superfamily)	0.40	110		
W02A11.4	uba-2	Degradation/protease	Ubiquitin-activating enzyme	0.57	70	0.91	32
W03H9.4		Unknown	Cactin	0.45	134		
W07E6.1		RNA synthesis	tRNA and rRNA cytosine-C5-methylase	0.64	66		
Y19D2B.1*		Cell architecture	α-Tubulin	0.80	92	0.45	40
Y38F1A.5	cyd-1	Cell cycle	Cyclin D	0.21	98	0.47	86
Y47D3A.6	tra-1	Transcription factor	GLI-family zinc-finger transcription factor	0.52	93	0.52	140
Y48A6C.5	pha-1	Unknown	Unknown	0.56	66	0.48	62
Y48G1A.5	imb-5	Cell architecture	Nuclear export receptor–importin β superfamily	0.64	42		
Y51H7C.6	cogc-4	Unknown	Conserved oligomeric Golgi complex component	0.47	110		
Y55F3AR.3		Protein synthesis	Chaperonin complex component, TCP-1 θ subunit	0.92	100		
Y59A8B.6		Nucleic acid binding	Splicing factor, snRNP-associated protein	0.61	98	0.48	50
Y65B4BR.5		Transcription factor	Nascent polypeptide-associated complex	0.38	90	0.28	78
Y71F9AM.4	cogc-3	Unknown	Conserved oligomeric Golgi complex component	0.57	98		
Y71G12B.11		Cell architecture	Talin	0.98	52		
Y92H12A.1†	src-1	Signaling	Src family kinase	0.60	40		
ZC504.4	mig-15	Signaling	Nck-interacting kinase, GCK family protein kinases	0.47	94	0.45	84
ZK1058.2	pat-3	Cell architecture	β Integrin	0.30	100		
ZK1151.1	vab-10	Cell architecture	Spectraplakin, microtubule-actin crosslinking factor	0.63	72		
ZK1236.3	sor-1	Unknown	Unknown	0.31	98	0.92	12
ZK328.5	npp-10	Cell architecture	Nuclear pore complex	0.45	100		
ZK430.7		RNA synthesis	Sof1-like rRNA processing protein	0.47	96	0.50	12
ZK637.8	unc-32	Cell architecture	Vacuolar H^+-ATPase V0 sector, subunit A	0.84	82		
ZK652.1	snr-5	RNA synthesis	Small nuclear ribonucleoprotein (snRNP)	0.79	96	0.48	71

The sequence name and genetic locus are unique identifiers for each *C. elegans* gene (see www.wormbase.org). A brief description based mainly on homology data derived from Wormbase is given. The functional classifications are based on previous gene assignments (Kamath et al., 2003) (Fig. 4). P0 defect indicates the proportion of gonad arms showing DTC migration defects by Nomarski microscopy 48 hours after hatching. For the F1 defects, young adult progeny of the P0 animals were analyzed 48 hours post hatching. *n* is the total number of gonad arms scored (typically two gonad arms per animal). 'Unknown' includes genes for which no functional data have been published, although some of these genes have similarity to known proteins. *Owing to sequence identity, RNAi clone may target more than one transcript (predicted by Wormbase). †RNAi-targeting vector was constructed for this study using primers listed in Table S4 in supplementary material.

example, proteins that mediate or contribute to cell-matrix interactions *ina-1*, *pat-3*, *unc-73*, talin, *src-1*, *ced-5*, *ced-10*, *gon-1* and *dig-1*, transcription factors *hlh-2* and *vab-3,* and Golgi transport proteins *cogc-2* and *cogc-3* were identified in our screen and confirmed to have DTC migration defects (Thomas et al., 1990; Greenstein et al., 1994; Baum and Garriga, 1997; Steven et al., 1998; Blelloch and Kimble, 1999; Nishiwaki, 1999; Reddien and Horvitz, 2000; Lee et al., 2001; Cram et al., 2003; Karp and Greenwald, 2004; Walker et al., 2004; Itoh et al., 2005; Lee et al., 2005; Kubota et al., 2006). Most of these studies analyzed loss-of-function alleles with phenotypes very similar to our RNAi phenotypes. Some published DTC migration genes were not isolated in this screen, probably because of the stringent nature of the primary screen or ineffective depletion of some genes by RNAi.

During secondary screening, three categories of DTC migration phenotypes were documented (Fig. 1D-G). The Type 1 category includes the most dramatic defects, which arise during the ventral phase of migration. DTCs fail to turn toward the dorsal side of the animal (Fig. 1D). In the second category (Type 2), the DTCs executed at least one supernumerary turn (Fig. 1E). The remainder of the defective animals fell into the Type 3 category and had phenotypes related to migration on the dorsal basement membrane. These dorsal phenotypes were the most common DTC migration defects observed. The major abnormalities included DTCs that failed to complete the dorsal phase of migration (Fig. 1F) or showed incorrect tracking along the dorsal surface (Fig. 1G). For the percentage of each type of defect for each RNAi experiment, see Table S3 in supplementary material.

The most severe defect in cell migration is Type 1, an early defect in which the DTC stops migrating while still on the ventral surface of the animal. Only 13 of the 99 genes had this depletion defect, including six genes encoding isoforms of cytoskeletal proteins actin or tubulin. GON-1/ADAMTS is known to be required for initiation of gonadogenesis (Blelloch and Kimble, 1999) and depletion of HLH-2, a basic helix-loop-helix transcription factor, causes failure of gonad arm extension (Karp and Greenwald, 2004). We observed severe ventral DTC migration defects with RNAi depletion of either GON-1 or HLH-2 (Fig. 2). Interestingly, depletion of the extracellular matrix (ECM) protein PPN-1/papilin caused a similar, very striking Type 1 defect (Fig. 2; Table S3 in supplementary material). Phenotypic similarities suggested that *ppn-1* and *gon-1* might be regulated by *hlh-2*. In support of this idea, we found sites matching the bHLH consensus binding sequence CANNTG (Kyriacou and Rosato, 2000) within 500 bp upstream of the *ppn-1* and *gon-1* coding regions. Both *gon-1* and *hlh-2* are expressed in the DTCs (Blelloch and Kimble, 1999; Karp and Greenwald, 2004). Examination of transgenic animals carrying a transcriptional fusion of *ppn-1::*GFP showed obvious expression in the DTC (Fig. 3A).

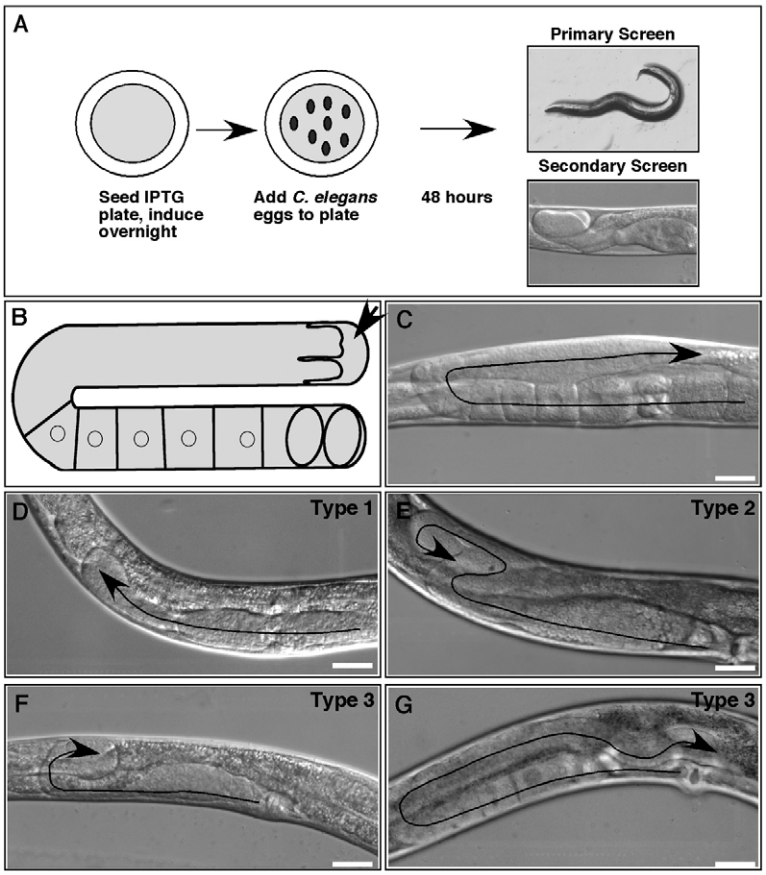

Fig. 1. Two-step screen to identify DTC migration defects. (A) Nematodes were cultured on bacterial strains from hatching to adulthood. The primary screen was performed 48 hours post hatching and young adults were scored for the presence of clear patches using a dissecting microscope. In the secondary screen, DTC migration paths were documented by Nomarski microscopy. (B) Diagram illustrating one arm of the hermaphrodite gonad. The DTC is indicated. Cuboidal cells are maturing oocytes. Ovals are fertilized embryos. (C-G) Nomarski images showing three types of defects. Treated *rrf-3(pk1426)* hermaphrodites were grown on *E. coli* HT115(DE3) carrying an empty vector (C) or RNAi targeting vectors for *act-1* (D), *ced-5* (E), *pat-3* (F), or *dyn-1* (G). Arrows indicate paths taken by DTCs. Anterior is to the left, ventral down in all images except D and F in which anterior is to the right. Bars, 20 μm.

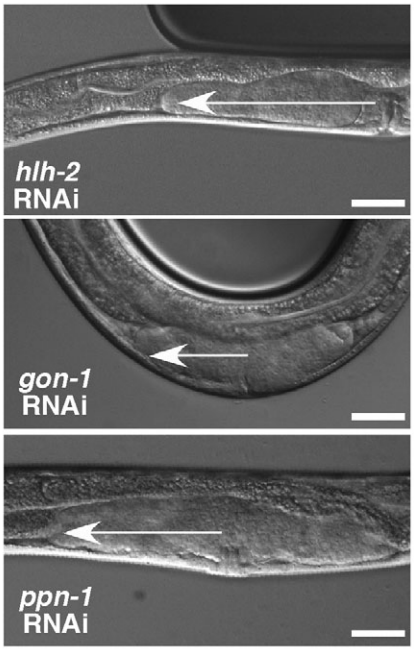

Fig. 2. Comparison of gonad defects with depletion of *hlh-2*, *ppn-1* and *gon-1*. Nomarski microscopy was used to visualize the gonads of age-matched hermaphrodites that were hatched and grown on bacteria carrying RNAi-targeting constructs for *hlh-2* (A), *ppn-1* (B) and *gon-1* (C). Arrows indicate lengths of paths taken by DTCs. Anterior is to the left, ventral is down in all images. Bars, 20 μm.

HLH-2 is required for that expression because GFP fluorescence was almost completely ablated in the DTC with *hlh-2* RNAi compared with control-treated animals (Fig. 3A,B). Expression of *gon-1* was also reduced with *hlh-2* RNAi (data not shown). These results identify two new gene targets, both encoding ECM proteins, for HLH-2.

Drosophila papilin binds to procollagen N-proteinase, which like GON-1 is an ADAMTS protein, and Kramerova et al. have proposed that papilin and GON-1 might interact in the *C. elegans* basement membrane (Kramerova et al., 2000). Expression of *ppn-1::*GFP was first observed in developing embryos, localized to the primordial gonad (Fig. 3C). Thus, *ppn-1* expression precedes *gon-1*, which is present between L2 and L4 stages (Blelloch and Kimble, 1999). Our results indicate that the gonad arms were somewhat more elongated with depletion of PPN-1 compared with GON-1 (see Fig. 2 arrows). On average, end-to-end lengths of gonad structures from *ppn-1* RNAi were twice the length of *gon-1* RNAi (arbitrary units ± s.d., 36.0±3.9 (n=32) vs 16.9±2.8 (n=19), respectively). This difference in phenotype allowed us to test the effects of combined loss of these two proteins. Double RNAi against *gon-1* and *ppn-1* gave the more dramatic *gon-1* phenotype (17.1±4.0, n=22). These data are consistent with a model in which PPN-1 and GON-1 are expressed as part of a developmental program that promotes migration of DTCs and is controlled by HLH-2. ECM deposition of PPN-1 by the DTCs could provide localized binding sites for GON-1, which is subsequently expressed at the time when DTC migration is initiated. In the absence of *gon-1* expression and proteolysis, DTC migration does not begin (Blelloch and Kimble, 1999). In the absence of PPN-1, secreted GON-1 might be inefficiently localized to the basement membrane and, therefore, would have limited contact with its targets for proteolysis. DTC migration would then cease shortly after the initiation step. We are currently testing this model.

Type 2 defects occur later than Type 1 defects and show extra turns resulting from problems in DTC navigation. These could be due to cell autonomous abnormalities in cell polarization or in responses to extracellular cues or to non-autonomous effects induced by incorrect deposition of the basement membrane. Type 2 was the smallest class of defects with only *vab-3* RNAi causing deficiencies in a majority of animals. Six other RNAi experiments had >30% Type 2 defects (Table S3, supplementary material) including the known

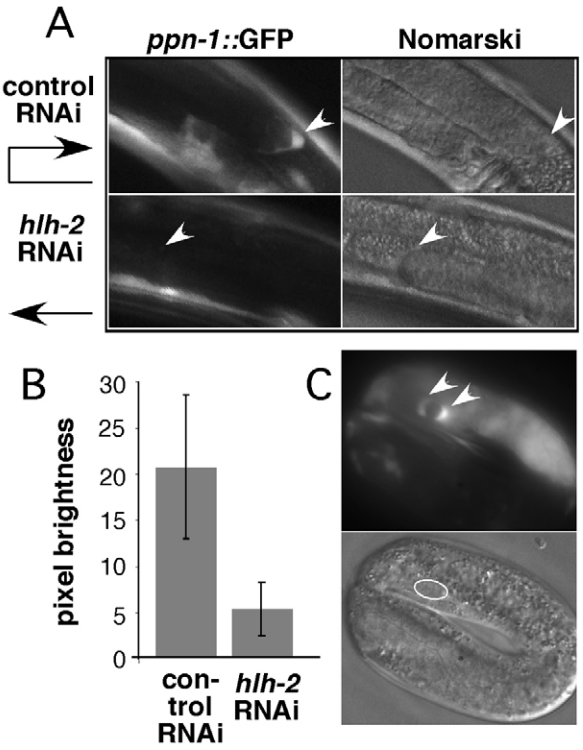

Fig. 3. *ppn-1* expression in the DTC and regulation by *hlh-2*. Eggs from *ppn-1::GFP* nematodes were hatched and grown on bacteria carrying an RNAi construct for *hlh-2* or on bacteria with a control plasmid. After 48 hours, Nomarski and fluorescence images were captured using identical exposure settings (A). DTC locations are indicated with arrowheads. DTC paths are diagrammed at the left. (B) Equal-sized ovals were centered around the DTCs on the Nomarski images and fluorescence intensities within the ovals were measured for ten animals from each condition using IPLab software. The average fluorescence ± s.d. for control and *hlh-2* RNAi experiments are shown. (C) An embryo expressing *ppn-1::GFP* shows expression in the DTC precursor cells Z1 and Z4 indicated by arrowheads in the fluorescence image. The gonad primordium is outlined in the Nomarski image.

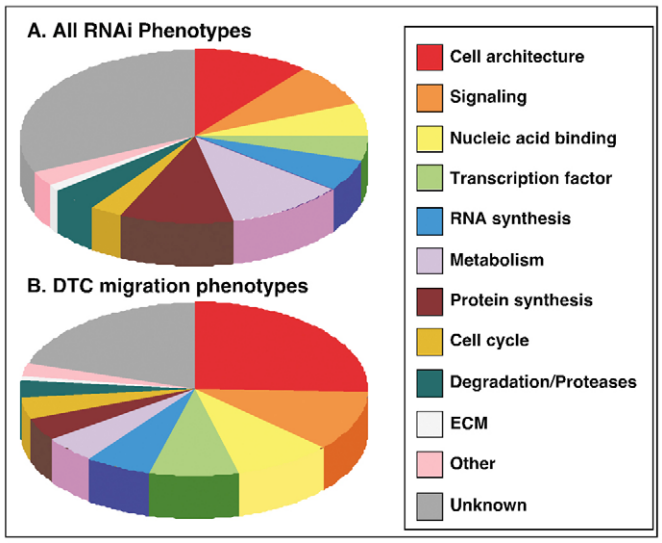

Fig. 4. Distributions of DTC migration genes by functional class. Functional classes for *C. elegans* genes as described previously (Kamath et al., 2003) are listed on the right. (A) The relative percentages for each functional class of genes that showed any RNAi phenotype are indicated. (B) Percentages for each functional class of those genes resulting in DTC phenotypes are shown. The functional class 'Nucleic acid binding' includes the categories RNA binding, DNA binding, NA binding and Chromatin. 'ECM' (extracellular matrix) includes collagens, *ppn-1* and *dig-1*.

regulators of DTC navigation *ced-5*/DOCK180 and *ced-10*/Rac (Reddien and Horvitz, 2000). Importantly, we also isolated genes not previously implicated in DTC pathfinding, including the cell architecture gene *vab-10*/spectraplakin, the transcription factors *icd-1*/bicaudal and *tra-1*, and the uncharacterized protein W07E6.1 (Table S3, supplementary material).

Although many types of genes participate in DTC migration, the cell architecture genes constituted the most abundant class (Fig. 4, Table 1), suggesting that the mechanism of migration of the DTC shares many of the general features of other migratory cells. Comparison of functional classes for the DTC migration genes (Fig. 4B) to those reported for all genes with RNAi phenotypes (Kamath et al., 2003) (Fig. 4A) shows a significantly higher proportion of cell architecture genes and a reduced proportion of the protein synthesis and metabolism gene classes in the DTC migration gene group. It is possible that some of the genes isolated by our RNAi screen might indirectly affect DTC migration; for example, depletion of an RNA splicing factor may have broad effects on gene expression. However, those genes expressed in the DTC itself or in the muscle cells that assemble the basement membrane on which the cells migrate are likely to be more directly involved in DTC migration. These genes are indicated in Table S3 in supplementary material. Importantly, the change in distribution of genes in these categories indicates that our set of genes is not a random sample drawn from all genes with RNAi phenotypes, but is a specific and unique set required for DTC migration.

We speculated that many of the 99 genes on our list might be working in concert to regulate DTC migration. Recently, a dataset predicting statistically significant, functional interactions between *C. elegans* genes has become available (Zhong and Sternberg, 2006). In this dataset, physical interaction, genetic interaction, subcellular localization and co-expression data all contribute to the significance of interaction between two genes. To illuminate the inter-relationships between DTC migration genes, we used a subset of these data (genes with probability of interaction $P>0.9$) (Zhong and Sternberg, 2006) and the network software Cytoscape (Shannon et al., 2003) to assemble a network of interacting genes (Fig. 5 and Fig. S1 in supplementary material). Red nodes represent 59 of the 99 DTC migration genes and green nodes are the minimal subset of interacting proteins necessary to depict pair-wise connections between each of the DTC migration genes. For identities of all nodes, see Fig. S1 in supplementary material. Assembly of these genes into a network revealed a cohesive set of genes that may work together to control cell migration.

Red and green nodes in the same vicinity of the network diagram (Fig. 5) are often functionally related or involved in

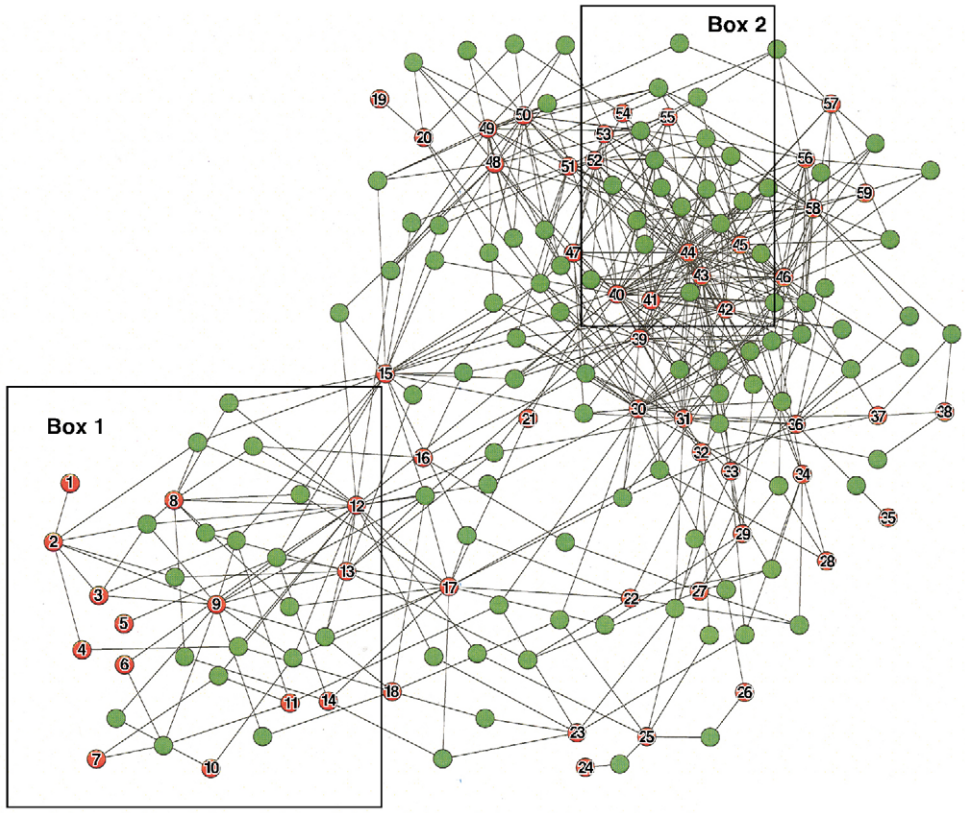

Fig. 5. Development of a DTC migration gene network. Red nodes represent the genes required for DTC migration isolated in this screen. Green nodes are a subset of interacting genes derived from a genome-wide prediction of *C. elegans* genetic and physical interactions (Zhong and Sternberg, 2006). For brevity, only red nodes are identified. For identities of all nodes see Fig. S1 in supplementary material. Identities of red nodes: (1) Y71G12B.11, (2) *pat-3*, (3) *unc-112*, (4) *vab-10*, (5) *gex-3*, (6) *ced-5*, (7) *ced-10*, (8) *erm-1*, (9) *ina-1*, (10) *sdn-1*, (11) *gon-1*, (12) *unc-73*, (13) *dyn-1*, (14) *mig-15*, (15) *act-1*, (16) *unc-32*, (17) *cdc-42*, (18) *vab-3*, (19) C16C10.6, (20) *uba-2*, (21) *let-2*, (22) *rab-8*, (23) *cbp-1*, (24) F32D1.2, (25) *rpl-11.1*, (26) *ppn-1*, (27) *arf-3*, (28) *cogc-4*, (29) *apc-2*, (30) *ruvb-1*, (31) *cct-1*, (32) W03H9.4, (33) F26F4.11, (34) *cogc-3*, (35) R53.6, (36) *mcm-7*, (37) *icd-1*, (38) Y65B4BR.5, (39) Y55F3AR.3, (40) *tba-1*, (41) *mix-1*, (42) *smc-4*, (43) *tba-2*, (44) *tba-4*, (45) ZK430.7, (46) H06I04.3, (47) F21C3.5, (48) *snr-5*, (49) T13H5.4, (50) Y59A8B.6, (51) F11A3.2, (52) *tbg-1*, (53) *tbb-2*, (54) *imb-5*, (55) *tbb-1*, (56) T04A8.3, (57) *npp-9*, (58) W07E6.1, (59) *npp-10*.

the same process. For example, the cell adhesion integrin receptor heterodimer INA-1/α and PAT-3/β forms an interaction cluster in this network with other proteins from our screen such as Y71G12B.11/talin, UNC-112/Mig-2, CED-10/Rac, ERM-1 and MIG-15/NIK (Fig. 5, box 1). Some of the green nodes in this cluster have also been implicated in cell adhesion or migration including laminin (*epi-1*) and perlecan (*unc-52*) ECM proteins, other Rho-family GTPases (*rho-1*, *rac-2*), and non-muscle myosin (*nmy-1*) (Fig. 1, supplementary material). The DTC signaling molecules *glp-1* and *lin-12* are also within this cluster. Many of these proteins are associated with the *C. elegans* muscle dense body complex and their orthologs are found in the vertebrate focal adhesion complex (Cox and Hardin, 2004). Integrins play an important role in the migration of many types of cells during development, wound healing and cancer metastasis (Guo and Giancotti, 2004), therefore, this cluster is likely to be relevant to cell migration in other systems. Tubulins and tubulin-interacting proteins form the other main cluster in the network (Fig. 5, box 2). The tubulin cluster is connected to the integrin cluster through multiple interacting proteins. Many links pass thorough the Rho-family GEF UNC-73 (Fig. 5, number 12) and the GTPase CDC-42 (Fig. 5, number 17). These interactions suggest that DTC migration provides an excellent model system for genetic and molecular analysis of integrin signaling during cell migration in vivo.

Comparing our data to screens conducted in other species should help to identify a conserved set of proteins required for cell migration. Two recent studies have identified multiple gene targets of Slbo, a CEBP family transcription factor necessary for migration of *Drosophila* border cells (Borghese et al., 2006; Wang et al., 2006). These results show overlap with our data in genes that regulate actin and microtubule cytoskeletal dynamics such as *vab-10*/shortstop, talin, and β integrin *pat-3*/myospheroid. Two other screens identified genes that affect morphology (Kiger et al., 2003) and lamellipodia extension (Rogers et al., 2003) of cultured *Drosophila* cells. There was some overlap between our data set and the genes identified in these *Drosophila* screens including *pat-3*/myospheroid, talin, *cdc-42*, *rho-1*, *mig-15*/misshapen, *src-1*, *ced-5*/myoblast city, *zen-4*/pavarotti and *dyn-1*/shibire.

Connections between DTC migration and mammalian cell migration are suggested by recent microarray analyses of metastasizing cells which provide an ‘invasion signature’ of

genes differentially regulated in these cells compared with cells in the primary tumor (Condeelis et al., 2005). Overlaps in the profile of genes necessary for tumor cell invasion and DTC migration include an ubiquitin-activating enzyme (UBA-2), a matrix metalloproteinase (GON-1), an ERM family member (ERM-1), members of the Ras-GTPase superfamily (CED-10, CDC-42 and RAB-8), kinesin (ZEN-4), integrin (PAT-3) and various α-tubulin genes (TBA-1, -2, -4). It seems likely that mammalian homologs of other DTC migration regulatory genes also play roles in migration and invasion by metastatic cells. It is noteworthy that certain genes have consistently emerged as essential migration components when DTC migration, *Drosophila* cell spreading and migration, and metastasis genes are compared. Further comparison with genome-wide cell migration screens along with detailed analyses of the network of proteins discovered in this study should help us better understand the multi-factorial processes that control cell migration.

Materials and Methods

Nematode strains

Strains were maintained as described (Hope, 1999) at 20°C. *E. coli* OP50 was used for maintenance of stocks, and the strain *E. coli* HT115(DE3) for RNAi. The wild-type nematode strain N2 Bristol was used for the primary screening of Chromosome I. All other RNAi experiments were conducted using the sensitized strain *rrf-3(pk1426)*. N2 and *rrf-3* strains were provided by the *Caenorhabditis* Genetics Center. BC15734[*dpy-5(e907)* I; sIs14164(*ppn-1*::GFP)] was constructed by the British Columbia *C. elegans* Gene Expression Consortium (McKay et al., 2003) and was obtained from the *Caenorhabditis* Genetics Center (CGC#6525).

RNAi

The RNAi-feeding protocol was conducted essentially as described (Cram et al., 2003; Kamath and Ahringer, 2003). In the primary screen, each clone was evaluated in 24-well plates containing NGM agar, 6 mM IPTG and 25 μg/ml carbenicillin. For the secondary screen, each culture was seeded on a 6-cm plate with the same components listed above. For both screens, eggs were released from gravid hermaphrodites using alkaline hypochlorite solution as described (Hope, 1999), transferred to plates seeded with HT115(DE3) bacteria expressing double-stranded RNA (dsRNA) and incubated at 23°C. These P0 animals were scored for clear patches by visual inspection using a dissecting microscope after 48 hours, and progeny (F1) were scored after 96 and 120 hours. For each batch of RNAi clones tested, pD129.36 (vector only) and *vab-10* or talin RNAi control wells were included. A phenotype was assigned to a well if any of the animals displayed clear patches. Animals that were small, arrested at larval stages, or had extruded intestines or gonads were not scored. The secondary screen was conducted by Nomarski microscopy using the method described (Cram et al., 2003). RNAi experiments resulting in ⩾30% of malformed gonad arms were scored as positive for DTC migration defects.

Double RNAi was performed by placing eggs on plates seeded with equal mixtures of two bacterial strains expressing different double-stranded RNAs: *gon-1*/*ppn-1*, *gon-1*/control bacteria and *ppn-1*/control bacteria. Gonad defects of young adult nematodes were checked by Nomarski microscopy.

Plasmid construction

To construct RNAi clones not available in the RNAi library (Kamath and Ahringer, 2003), primers were designed to the predicted cDNA sequence and used for RT-PCR amplification with N2 total RNA as the template. Values in the primer names indicate the position on the cDNA relative to the ATG. Most primers included *Nhe*I and *Hin*dIII sites at the 5′ and 3′ ends, respectively, and these sites were used to clone the PCR product into pPD129.36 vector. Primer sequences are presented in Table S4 in supplementary material.

PCR validation of clones

To validate RNAi clones taken from the library (Kamath and Ahringer, 2003), T7 primers were used in PCR reactions to amplify the insert. The predicted size of the insert was compared with the PCR amplified insert. In cases of discrepancy, the identity of the RNAi target was confirmed by sequencing. All sequences were found to be correct except for well I-1E13, which we found to target F01G12.5/*let-2* and well IV-8B19, which targets F56A3.3/*npp-6*.

Analysis of *ppn-1*::GFP expression

Nematodes were photographed with a Nikon TE-2000U microscope as described previously (Cram et al., 2003). RNAi for *hlh-2* was performed as described above using *ppn-1*::GFP (BC15734) nematodes. After hatching, nematodes were grown on *hlh-2* RNAi or control bacteria for 48 hours at 23°C. The distal ends of gonads from RNAi-treated nematodes were photographed using a 40× objective and a 0.1-second exposure. Corresponding Nomarski images were used to center an oval around the end of each gonad arm. GFP brightness per pixel within each oval was quantified using Scanalytics IPLab software.

Network construction

The interaction network (Fig. 5) depicts functional interactions between *C. elegans* genes using a subset of the interaction data reported by Zhong and Sternberg (Zhong and Sternberg, 2006). The interaction data were mined for each of the 99 genes from our DTC migration screen (Table 1) and a list of all interacting genes/nodes with a probability of interaction $P>0.9$ was assembled. This list included 1670 interactions. Non-DTC genes with only one interaction were removed from the list. In some cases, there were multiple parallel sets of genes linking the same pair of DTC genes and all but one link was removed from the list. The resulting list of interacting pairs included 554 interactions. The network software Cytoscape (Shannon et al., 2003) was used to assemble a network of interacting genes from this list of interacting pairs.

The authors thank Shanisha Gordon and Nicolette Wangler for technical assistance, Maria Martynovsky for sharing data, and Douglas Finkbeiner and Chris Meighan for critical reading of the manuscript. This work was supported by grants from the National Institutes of Health GM059383 (J.E.S.), the Damon Runyon Cancer Research Fund and the Robert Black Charitable Foundation (1706-02) (E.J.C.) and the NIGMS Cell Migration Consortium (U54 GM 064346).

References

Baum, P. D. and Garriga, G. (1997). Neuronal migrations and axon fasciculation are disrupted in ina-1 integrin mutants. *Neuron* **19**, 51-62.

Blelloch, R. and Kimble, J. (1999). Control of organ shape by a secreted metalloprotease in the nematode Caenorhabditis elegans. *Nature* **399**, 586-590.

Borghese, L., Fletcher, G., Mathieu, J., Atzberger, A., Eades, W. C., Cagan, R. L. and Rorth, P. (2006). Systematic analysis of the transcriptional switch inducing migration of border cells. *Dev. Cell* **10**, 497-508.

Condeelis, J., Singer, R. and Segall, J. E. (2005). The great escape: when cancer cells hijack the genes for chemotaxis and motility. *Annu. Rev. Cell Dev. Biol.* **21**, 695-718.

Cox, E. A. and Hardin, J. (2004). Sticky worms: adhesion complexes in C. elegans. *J. Cell Sci.* **117**, 1885-1897.

Cram, E. J., Clark, S. G. and Schwarzbauer, J. E. (2003). Talin loss-of-function uncovers roles in cell contractility and migration in C. elegans. *J. Cell Sci.* **116**, 3871-3878.

Greenstein, D., Hird, S., Plasterk, R. H., Andachi, Y., Kohara, Y., Wang, B., Finney, M. and Ruvkun, G. (1994). Targeted mutations in the Caenorhabditis elegans POU homeo box gene ceh-18 cause defects in oocyte cell cycle arrest, gonad migration, and epidermal differentiation. *Genes Dev.* **8**, 1935-1948.

Guo, W. and Giancotti, F. G. (2004). Integrin signalling during tumour progression. *Nat. Rev. Mol. Cell Biol.* **5**, 816-826.

Hesselson, D., Newman, C., Kim, K. W. and Kimble, J. (2004). GON-1 and fibulin have antagonistic roles in control of organ shape. *Curr. Biol.* **14**, 2005-2010.

Hope, I. A. (ed.) (1999). *C. elegans, A Practical Approach* (*The Practical Approach Series*). Oxford: Oxford University Press.

Itoh, B., Hirose, T., Takata, N., Nishiwaki, K., Koga, M., Ohshima, Y. and Okada, M. (2005). SRC-1, a non-receptor type of protein tyrosine kinase, controls the direction of cell and growth cone migration in C. elegans. *Development* **132**, 5161-5172.

Kamath, R. S. and Ahringer, J. (2003). Genome-wide RNAi screening in Caenorhabditis elegans. *Methods* **30**, 313-321.

Kamath, R. S., Fraser, A. G., Dong, Y., Poulin, G., Durbin, R., Gotta, M., Kanapin, A., Le Bot, N., Moreno, S., Sohrmann, M. et al. (2003). Systematic functional analysis of the Caenorhabditis elegans genome using RNAi. *Nature* **421**, 231-237.

Karp, X. and Greenwald, I. (2004). Multiple roles for the E/Daughterless ortholog HLH-2 during C. elegans gonadogenesis. *Dev. Biol.* **272**, 460-469.

Kiger, A. A., Baum, B., Jones, S., Jones, M. R., Coulson, A., Echeverri, C. and Perrimon, N. (2003). A functional genomic analysis of cell morphology using RNA interference. *J. Biol.* **2**, 27.

Kramerova, I. A., Kawaguchi, N., Fessler, L. I., Nelson, R. E., Chen, Y., Kramerov, A. A., Kusche-Gullberg, M., Kramer, J. M., Ackley, B. D., Sieron, A. L. et al. (2000). Papilin in development; a pericellular protein with a homology to the ADAMTS metalloproteinases. *Development* **127**, 5475-5485.

Kubota, Y., Kuroki, R. and Nishiwaki, K. (2004). A fibulin-1 homolog interacts with an ADAM protease that controls cell migration in C. elegans. *Curr. Biol.* **14**, 2011-2018.

Kubota, Y., Sano, M., Goda, S., Suzuki, N. and Nishiwaki, K. (2006). The conserved oligomeric Golgi complex acts in organ morphogenesis via glycosylation of an ADAM protease in C. elegans. *Development* **133**, 263-273.

Kyriacou, C. P. and Rosato, E. (2000). Squaring up the E-box. *J. Biol. Rhythms* **15**, 483-490.

Lee, J., Li, W. and Guan, K. L. (2005). SRC-1 mediates UNC-5 signaling in Caenorhabditis elegans. *Mol. Cell. Biol.* **25**, 6485-6495.

Lee, M., Cram, E. J., Shen, B. and Schwarzbauer, J. E. (2001). Roles for beta(pat-3) integrins in development and function of Caenorhabditis elegans muscles and gonads. *J. Biol. Chem.* **276**, 36404-36410.

Lehmann, R. (2001). Cell migration in invertebrates: clues from border and distal tip cells. *Curr. Opin. Genet. Dev.* **11**, 457-463.

McKay, S. J., Johnsen, R., Khattra, J., Asano, J., Baillie, D. L., Chan, S., Dube, N., Fang, L., Goszczynski, B., Ha, E. et al. (2003). Gene expression profiling of cells, tissues, and developmental stages of the nematode C. elegans. *Cold Spring Harb. Symp. Quant. Biol.* **68**, 159-169.

Merz, D. C., Zheng, H., Killeen, M. T., Krizus, A. and Culotti, J. G. (2001). Multiple signaling mechanisms of the UNC-6/netrin receptors UNC-5 and UNC-40/DCC in vivo. *Genetics* **158**, 1071-1080.

Nishiwaki, K. (1999). Mutations affecting symmetrical migration of distal tip cells in Caenorhabditis elegans. *Genetics* **152**, 985-997.

Nishiwaki, K., Kubota, Y., Chigira, Y., Roy, S. K., Suzuki, M., Schvarzstein, M., Jigami, Y., Hisamoto, N. and Matsumoto, K. (2004). An NDPase links ADAM protease glycosylation with organ morphogenesis in C. elegans. *Nat. Cell Biol.* **6**, 31-37.

Reddien, P. W. and Horvitz, H. R. (2000). CED-2/CrkII and CED-10/Rac control phagocytosis and cell migration in Caenorhabditis elegans. *Nat. Cell Biol.* **2**, 131-136.

Rogers, S. L., Wiedemann, U., Stuurman, N. and Vale, R. D. (2003). Molecular requirements for actin-based lamella formation in Drosophila S2 cells. *J. Cell Biol.* **162**, 1079-1088.

Shakir, M. A. and Lundquist, E. A. (2005). Analysis of cell migration in Caenorhabditis elegans. *Methods Mol. Biol.* **294**, 159-173.

Shannon, P., Markiel, A., Ozier, O., Baliga, N. S., Wang, J. T., Ramage, D., Amin, N., Schwikowski, B. and Ideker, T. (2003). Cytoscape: a software environment for integrated models of biomolecular interaction networks. *Genome Res.* **13**, 2498-2504.

Steven, R., Kubiseski, T. J., Zheng, H., Kulkarni, S., Mancillas, J., Ruiz Morales, A., Hogue, C. W., Pawson, T. and Culotti, J. (1998). UNC-73 activates the Rac GTPase and is required for cell and growth cone migrations in C. elegans. *Cell* **92**, 785-795.

Thomas, J. H., Stern, M. J. and Horvitz, H. R. (1990). Cell interactions coordinate the development of the C. elegans egg-laying system. *Cell* **62**, 1041-1052.

Walker, D. S., Ly, S., Gower, N. J. and Baylis, H. A. (2004). IRI-1, a LIN-15B homologue, interacts with inositol-1,4,5-triphosphate receptors and regulates gonadogenesis, defecation, and pharyngeal pumping in Caenorhabditis elegans. *Mol. Biol. Cell* **15**, 3073-3082.

Wang, X., Bo, J., Bridges, T., Dugan, K. D., Pan, T. C., Chodosh, L. A. and Montell, D. J. (2006). Analysis of cell migration using whole-genome expression profiling of migratory cells in the Drosophila ovary. *Dev. Cell* **10**, 483-495.

Zhong, W. and Sternberg, P. W. (2006). Genome-wide prediction of C. elegans genetic interactions. *Science* **311**, 1481-1484.